HfB_2-SiC-$MoSi_2$ oxidation resistance coating fabricated through in-situ synthesis for SiC coated C/C composites

Peipei Wang[1], Hejun Li[1,*], Xuanru Ren[2], Ruimei Yuan[1], Xianghui Hou[3], Yulei Zhang[1,*]

1 *State Key Laboratory of Solidification Processing, Carbon/Carbon Composites Research Center, Northwestern Polytechnical University, Xi'an Shaanxi 710072, PR China*

2 *College of Material Science and Engineering, China University of Mining and Technology, Xuzhou, Jiangsu 221116, PR China*

3 *Faculty of Engineering, University of Nottingham, Nottingham NG7 2RD, United Kingdom*

Abstract

A brand new HfB_2-SiC-$MoSi_2$ coating was fabricated to protect carbon/carbon (C/C) composites with inner SiC coating from oxidation, which was prepared by in-situ synthesis. In this paper, the C/C substrate with the protection of the HfB_2-SiC-$MoSi_2$/SiC coating could resist oxidation in 1773 K air for 408 h. The double coating also presented expected oxidation protection performance at dynamic oxidation environment. In the test process, the surface coating was oxidized to form a self-sealing silicate glass layer containing HfO_2 and $HfSiO_4$, which could hinder crack propagation in coating.

Keywords: C/C composites; Oxidation; Surface analysis; Heat treatment

* Corresponding author. Tel.: +86 29-88492272 (H. Li), +86 29-88491834 (Y. Zhang); fax: +86 29-88492642 (H. Li), : +86 29-88492642 (Y. Zhang).
E-mail address: lihejun@nwpu.edu.cn (H. Li), zhangyulei@nwpu.edu.cn (Y. Zhang).

1. Introduction

In the fields of aeronautics and astronautics, carbon/carbon (C/C) composites are a kind of the most promising thermal structural materials [1-4], which are noted for their outstanding mechanical properties from low temperature to very high temperature, for instance, high creep resistance, low efficient of thermal expansion and suitable resistance to thermal shock [5-7]. Just because there are so many special characteristics, they are preferable material for aeronautical and space application, such as turbine engines, leading edges of reentry vehicles, rocket nozzle and so on [8]. But their wide applications are limited owing to the easy oxidation above 723 K in atmospheric conditions [9-10]. The multilayer protective layer is a pivotal strategy to solve the problem [11-12]. SiC coating has low thermal expansion coefficient and appropriate compatibility with C/C composites. It can also form dense and continuous SiO_2 glass layer during oxidation, so SiC is considered to be the inner coating of C/C composites. However, SiO_2 glass layer is volatile more than 1500, which can form some defects in the glass layer.

Recently, UHTCs of borides have attracted many attentions because of their high melting point, high hardness, excellent oxidation resistance performance and good chemical stability [13-15]. In addition, their oxides also present as the inlay in SiO_2 glass, which will improve the stability of the silicate glass and block oxygen into substrate [16-17]. It is helpful to decrease the generation of the cracks, and lessen the penetration of oxygen, which are all conducive to increase the anti-oxidation of the sample and then protect C/C substrate better. Therefore, introducing transition-metal borides into the SiC coatings is promising to broaden their application prospect.

Among the transition metal borides ceramic, hafnium diboride (HfB_2) [18-20] as one of promising candidates has attracted much attention in recent years, which has a series of unexceptionable performances, for instance, excellent resistance to oxidation and thermal shock. The method of in-situ synthesis is easy to fabricate the UHTCs borides at the lower temperature [21]. During the preparation process, many reactions may occur to generate the desired phases.

In this research, the Si, C, B_2O_3, HfO_2 and Mo powders as raw materials prepared the UHTCs HfB_2-SiC-$MoSi_2$ oxidation protective layer through in-situ synthesis on the surface of C/C composites with SiC coating. Furthermore, the dynamic anti-oxidation of HfB_2-SiC-$MoSi_2$ coating from room temperature to 1673 K had been investigated. Meanwhile, the microstructure, oxidation protection behavior and mechanism of the samples at 1773 K also were investigated.

2. Experimental procedures

The oxidation protective coatings were applied on 2-D C/C composites substrates, which were cut into little specimens ($8\times8\times8$ cm^3). The density of the C/C substrate was 1.70 g/cm^3. Before applying the coatings, the specimen was polished first and then ultrasonically cleaned. The coating contained SiC layer and HfB_2-SiC-$MoSi_2$ layer was applied on the C/C substrate. The pack cementation technique with Graphite (20-40 wt.%) and Si (60-80 wt.%) as raw materials were used for fabricating the inner SiC coating [21]. While the raw materials of B_2O_3 (10-25 wt.%), graphite (3-15 wt.%), HfO_2 (25-40 wt.%), Mo (5-10 wt.%) and Si (40-60 wt.%) powders could fabricate the outer HfB_2 (30 wt.%)-SiC (58 wt.%)-$MoSi_2$ (12 wt.%) coating through in-

situ synthesis. All the specimens and raw powders were placed in the graphite crucible with a heat treatment of heating up 5-10 K/min, then thermal insulation for 2 hours at 2373 K in normal argon atmosphere.

The isothermal oxidation test and thermo gravimetric analysis (TGA) test was used for researching the oxidation resistance of the samples. An isothermal oxidation test was implemented in 1773 K air and the samples were placed in an oxidation furnace. The samples were weighed by an analytical balance whose sensitivity is ± 0.1 mg. The samples were taken out of the oxidation furnace at set intervals during oxidation. As time went on, the accumulated weight alterations rates were calculated. The TGA test with the heating rate of 10 K/min measured the dynamic oxidation resistance of the specimens whose weight alterations were recorded by thermogravimetry mode in air atmosphere from room temperature to 1673 K. The crystalline structure, microstructures and elemental distribution could be analyzed by X-ray diffraction (XRD), scanning electron microscope (SEM) and energy dispersive spectroscopy (EDS), respectively. And the time taken of each point for EDS data collection was 60 s.

3. Experimental results and discussion

3.1 Microstructure of the coatings

An illustration diagram of the preparation process of outer HfB_2-SiC-$MoSi_2$ layer is shown in Fig.1 and it can be divided into four steps. At first, according to a certain proportion, the raw materials of Si, C, HfO_2, B_2O_3 and Mo powders were used for packing the C/C with inner SiC coating, thereby making the samples surrounded by these powders in all directions. Then, during the heat-treatment of the samples at 2373 K, carbothermal reduction reaction as well as the solid reaction would occur among the raw materials, which would form the HfB_2, SiC and

$MoSi_2$ particles. Next, during the process of the in-situ reaction, due to the low melting point of silicon, molten silicon was formed, which would be helpful to form the outer HfB_2-SiC-$MoSi_2$ coating. In addition, owing to the fluidity of the silicon melt, the formed coating materials were carried to penetrate into the inner coating, thus strengthening the bonding between inner and outer coating. Finally, the HfB_2-SiC -$MoSi_2$/SiC double coating was prepared on C/C substrates.

The XRD pattern of HfB_2-SiC-$MoSi_2$ coating is shown in Fig.2. The HfB_2-SiC-$MoSi_2$ coating comprises HfB_2, β-SiC, α-SiC and $MoSi_2$ phases, they are all the desired products. The HfB_2 phase is obtained by the in-situ carbothermal reduction reaction to reduce HfO_2 using B_2O_3 and graphite. The SiC phase is made by Si and C powders, while the $MoSi_2$ phase is made by Si and Mo powders with the solid reaction. All phases are acquired in the process of heat-treatment, which proves the superiority of this method. The reactions can be drawn as follows:

$$HfO_2\ (s) + B_2O_3\ (s) + 5C\ (s) \rightarrow HfB_2\ (s) + 5CO\ (g) \quad (1)$$

$$Si\ (g) + C\ (s) \rightarrow SiC\ (s) \quad (2)$$

$$2Si\ (g) + Mo\ (s) \rightarrow MoSi_2\ (s) \quad (3)$$

The backscatter micrographs of the HfB_2-SiC-$MoSi_2$ coating are shown in Fig.3. As shown in Fig.3 (a), the outer coating is dense with a lot of white and grey particles distributed on its surface. Fig.3 (b) shows a higher magnification than Fig.3 (a), from which the coating includes of three kinds of grains (white, black and grey phases). Through XRD and spot analyses of EDS (Fig.3 (c)), the different grains are confirmed as HfB_2 (white phase), SiC (black phase)

and $MoSi_2$ (grey phase). The SiC grains bond closely and few gaps can be seen among them. In addition, the HfB_2 and $MoSi_2$ grains mainly exist in the interspaces among SiC grains, which indicates that the outer coating is formed by the combination of the three kinds of grains. The close bonding among the grains is conducive to establish a barrier to effectively hinder the penetration of oxygen, thus decreasing the possibility of oxidation occurred at the C/C substrate.

In Fig.4 (a), the cross-section backscatter micrograph of the HfB_2-SiC-$MoSi_2$/SiC coated C/C is analyzed. The double layer coating has a thickness about 200-310μm, and no penetrating crack or obvious hole appears. In addition, some coating materials actually penetrate into substrate through the defects, and the bonding strength of the matrix and coating is enhanced. The high magnification of Fig.4 (a) is shown in Fig.4 (b). No distinct interface of double coating can be observed, which shows a close combination between two coatings. Furthermore, some white HfB_2 particles can be found in the inner coating owing to the penetration of the outer coating materials during preparing outer coating. Therefore, the penetration of outer coating materials into the inner coating will contribute to pad the defects of the inner coating and build a strong combination between the double coatings. As shown in Fig.4 (c), the inner SiC coating combines closely with C/C substrate and no distinct gap was observed between them. Owing to the penetration of the coating materials into the voids of substrate, some carbon fibers were wrapped as Fig.4 (d). Through spot EDS analyses (Fig.4 (e)), the materials can be confirmed as SiC. Fig.4 (f) presents the line analyses of HfB_2-SiC-$MoSi_2$ coating. Four elements are detected which present different trends, and the curves can be divided into two parts. The Si element is widespread in the inner and outer coating and most of the C element exists in the inner part, the Hf and Mo element is mainly present in 130-330 μm. In summary, the coating

presents HfB_2-SiC-$MoSi_2$/SiC double layer structure, and it is coincident with our prospective coating.

3.2 The 1773 K isothermal oxidation test of HfB_2-SiC-$MoSi_2$/SiC coating

The 1773 K isothermal oxidation test in air was carried out to survey the oxidation resistance of the HfB_2-SiC-$MoSi_2$/SiC coated C/C composites as shown in Fig.5. The oxidation curve of C/C with SiC coating exhibits a rapid increase trend. The weight loss of the samples reaches to 4.15 % after testing 54 h, which presents a finite oxidation resistance. While after applying the outer HfB_2-SiC-$MoSi_2$ coating, the weight loss rate of the samples drops to 0.76 % after testing 408 h, which indicates that the oxidation resistance of the coating is further improved. Furthermore, The C/SiC/$MoSi_2$-Si coatings prepared by zhang et al. [23] can protect C/C for 300 h under the same conditions with weight loss 1.4 %. It proves the introduction of HfB_2 phase to effectively increase the oxidation resistance of silicon-based ceramic coating.

XRD pattern of C/C with HfB_2-SiC-$MoSi_2$/SiC coating after oxidation 408 h is shown in Fig.6. After a period of time of oxidation, many oxidation products are generated. Strong SiO_2 peaks are detected in XRD, which means the generation of the silicate glass. Because of the self-sealing performance, the formed silicate glass can fill some flaws of coating and protect C/C substrate. HfO_2 peaks appear, which is the solid oxidation product of HfB_2. HfO_2 is a stable transition metal oxide, whose presence will improve the glass layer stability and viscosity. Except SiO_2 and HfO_2 peaks, $HfSiO_4$ peak can also be found, which is generated due to the

reaction of SiO_2 and HfO_2. $HfSiO_4$ phase is thermal stable with a high melting point (>2900), whose formation will enhance the oxidation protection of the glass layer effectively.

According to Fig.7 (a), the surface backscatter micrograph of HfB_2-SiC-$MoSi_2$/SiC coated C/C after oxidation 408 h at 1773 K is shown. During experiment, the specimens were removed at set intervals, which would generate great temperature difference, and create micro-cracks. Although an intact silicate glass layer over the coating, some micro-cracks can still form owing to the thermal expansion coefficients difference with coating, it can provide a way for oxygen into substrate, so increasing the likelihood of oxidation occurred at inner. And a small amount of bubbles exist in the glass layer. In addition, a mass of white grains consist in the silicate glass layer. The magnification of the white particles is shown in Fig.7 (b). Parts of the white particles are in fact embedded in the black glass layer. By EDS analyse (shown in Fig.7 (d)), the black layer is confirmed as SiO_2 glass, and the white particles are composed of HfO_2 and $HfSiO_4$. Since the SiO_2 glass possesses fluidity at high temperature and the $HfSiO_4$ phase is formed owing to the reaction between the SiO_2 and HfO_2, the HfO_2 and $HfSiO_4$ grains are embedded in the silicate glass through a close chemical bonding, which presents as immiscible phases in SiO_2 glass and increases its viscosity. As shown in Fig.7 (c), crack deflecting or termination appears in the surrounding of the white grains, it might be caused by the "pinning effect" played by HfO_2 and $HfSiO_4$ grains, thus beneficial to expending the cracks energy, and effectively promoting the oxidation resistance of samples.

Fig.8 shows the cross-section backscatter micrograph of HfB_2-SiC-$MoSi_2$/SiC coating after testing for 408 h. In Fig.8 (a), no penetration crack can be observed in the section, which proves

its good oxidation resistance. Fig.8 (b) presents the magnification of Fig.8 (a) after oxidation. Although some holes are existed because of the coating being oxidized, a large part of the coating is still very dense. Besides, plentiful white grains can still be found on the surface. Through EDS analysis (Fig.8 (f)), the white particles in the outer part of the coating can be recognized as the solid oxidation products of $HfSiO_4$, while the white particles in the inner part of the coating are the un-reacted HfB_2. Therefore, the external of the coating is oxidized primarily. The magnification of the outer part of the coating is shown in Fig.8 (c). The outer part of the coating consists of two zones. One zone is the loose and porous region, caused from oxidation. Another near the substrate is the fine and close region, thus shows an un-reacted zone. Fig.8 (d) shows the magnification of Fig.8 (a) part B. Part of the carbon fibers wrapped by coating materials can be found from it. Through EDS analyses (Fig.8 (f)), O element is detected in the SiC coating materials, which manifests SiC being oxidized due to the penetration of oxygen. However, owing to the protection of SiC, the wrapped carbon fibers are not oxidized. In Fig.8 (e), due to the oxidation of carbon, many holes exist in the substrate. According to the different oxidation levels, the substrate is divided into two oxidation zones, one zone is higher oxidation zone, and another is lower oxidation zone. In the former, the substrate is very dense, mainly composed of carbon fibers and pyrolytic carbon, therefore, more voids can be observed due to the fast oxidation of carbon. While in the lower oxidation zone, many coating materials appears in the substrate because of the penetration of them during preparing the inner SiC coating, which can be good for protecting the C/C substrate, therefore, fewer voids are formed.

3.3 Dynamic oxidation test of HfB_2-SiC-$MoSi_2$ coating

The Dynamic oxidation test of the HfB_2-SiC-$MoSi_2$/SiC coated C/C is investigated in a wide temperature range from room temperature to 1673 K with the heating rate of 10 K/min as shown

in Fig.9. After the TGA experiment, the weight losses rates of the C/C substrates coated with single coating and double coating are 19.65 % and 10.29 %, respectively. The coated samples in the oxidation process of a wide temperature range can be divided into three stages as shown in Fig.9 (a): A stage (room temperature-800K), B stage (800 K-1400 K) and C stage (1400 K-1673 K). At A stage, neither of two kinds of samples loses weight, but shows a slight weight gain phenomenon. The high magnification of B stage is shown in Fig.9 (b). The single SiC coating displays weak oxidation resistance above 800 K, but with the modification of HfB_2 and $MoSi_2$ phases, whose oxidation protection is observably promoted, it reveals the remarkable oxidation resistance of HfB_2 in a wide temperature range. In general, silica-based coating can form fluid SiO_2 glass at temperature above 1400 K, thus it has the expected oxidation protective effect in this temperature range, but the SiO_2 glass layer cannot protect substrates effectively from 800 K to 1473 K, which causes large weight loss. Owing to the oxidation of HfB_2 phase, B_2O_3 is a crucial oxidation product in the range from 800K to 1400 K, which can heal some defects in the coating and provide effective oxidation protection before the generation of the SiO_2 glass. The high magnification of C stage is shown in Fig.9 (c). When the temperature reaches the oxidation protection range of silicon-based ceramic, the vast defects have existed in the coating and substrate, thus the SiC coated sample continues losing weight. However, the TGA curve of HfB_2-SiC-$MoSi_2$/SiC coated C/C flattens out gradually owing to the formation of Hf-Si-O glass. In addition, the existence of $MoSi_2$ phase is conducive to form denser SiO_2 glass layer and reduce the consumption of SiO_2 glass [22], which can preferably inhibit the

entrance and spread of oxygen. Therefore, with the coexistence of HfB_2 and $MoSi_2$ phases, the samples present anticipant oxidation resistance in the TGA test.

3.4 Anti-oxidation mechanism of the HfB_2-SiC-$MoSi_2$/SiC coating

In order to analysisof oxidation mechanism, a schematic diagram of the HfB_2-SiC-$MoSi_2$/SiC coated C/C is shown as Fig.10. Before oxidation, the double coatings including SiC and HfB_2-SiC-$MoSi_2$ coating are applied on C/C specimens to prevent oxidation (Fig.10 (a)). The C/C substrates covers with coatings are exposed to the oxygen atmosphere at 1773 K. Under the attack of the oxygen, the coating materials can react with oxygen firstly, basing on the reactions (4)-(11).

$$SiC\ (s) + 2O_2\ (g) \rightarrow SiO_2\ (s) + CO_2\ (g) \quad (4)$$
$$2SiC\ (s) + 3O2\ (g) \rightarrow 2SiO2\ (s) + 2CO\ (g) \quad (5)$$
$$2HfB2\ (s) + 5O2\ (g) \rightarrow 2HfO2\ (s) + 2B2O3\ (s) \quad (6)$$
$$2MoSi2\ (s) + 7O2\ (g) \rightarrow 2MoO3\ (g) + 4SiO2\ (s) \quad (7)$$
$$HfO2\ (s) + SiO2\ (s) \rightarrow HfSiO4\ (s) \quad (8)$$
$$2SiO2\ (s) + SiC\ (s) \rightarrow 3SiO\ (g) + CO\ (g) \quad (9)$$
$$2C\ (s) + O2\ (g) \rightarrow 2CO\ (g) \quad (10)$$
$$C\ (s) + O2\ (g) \rightarrow CO2\ (g) \quad (11)$$

As shown in Fig.10 (b), at the initial period of oxidation, although many kinds of solid products generate, such as SiO_2, B_2O_3 and HfO_2, they can't form a complete protective layer to block oxygen into the coating. In addition, some gas byproducts are also generated, which will be released from the sample and result in the weight loss. The SiC inner coating is oxidized to produce SiO gas (reaction (9)), which can consume the SiO_2 protective layer, and cannot be removed quickly enough by the bubble migration. Moreover, it will prompt that the SiO_2 glass generates bubbles and defects, which cannot completely self-cure. The oxidation of $MoSi_2$

phase can produce moreSiO_2, which means the formation of more dense of SiO_2 glass layer offering the expected self-cure ability. Accompanied by the longer test time, more SiO_2 glass are generated due to the oxidation of SiC and $MoSi_2$, thus rapidly forming a continuous silicate glass layer, which can cover the defects and block the diffusion path of oxygen [23-24]. Owing to the fluidity of the SiO_2 glass layer, the formed HfO_2 particles are embedded in the silicate glass, thereby presenting as immiscible phases in it and increasing its viscosity and stability. Based on reaction (8), $HfSiO_4$ particles are formed by the reaction of SiO_2 and HfO_2 (Fig.10 (c)), which will serve as the reinforcing phase with HfO_2 in the silicate glass layer. In Fig.10 (d), because the volume change of coating and glass layer is different under unit temperature variation, some micro-cracks are formed [25-26]. However, because of the "pinning effect" of HfO_2 and $HfSiO_4$ particles in the silicate glass layer, the formed microcracks are forced to deflect and terminate, which decreases the size of cracks and effectively increase the oxidation protection of glass layer [27-28]. After a long time oxidation (Fig.10 (e)), some oxygen penetrates matrix and C/C is oxidized, accordingly some voids are formed. Moreover, some carbon fibers wrapped by the penetrated coating materials are protected from the oxidation. However, although a fraction of substrate is oxidized, the weight loss of the sample is only 0.76% after oxidation 408 h at 1773 K in air and 10.29% after TGA test, which shows its remarkable oxidation protection ability.

4. Conclusions

The in-situ synthesis was used for fabricating outer HfB_2-SiC-$MoSi_2$ coating to apply on C/C with inner SiC coating. The double layer coating with the thickness about 200-310 μm could

protect C/C composites 408 h at 1773 K with 0.76 % weight loss. The dense and continuous silicate glass layer concluding HfO_2 and $HfSiO_4$ particles was formed during the oxidation. The HfO_2 and $HfSiO_4$ particles were inlayed in SiO_2 glass, they could enhance its stability and viscosity and decrease the flaw size. By the end of oxidation test, the oxidation of the coating primarily occurred in coating external, and C/C was intact protected.

Acknowledgements

This work has been supported by the National Natural Science Foundation of China under Grant No. 51272212, 51672223 and 51521061, the "111" project under Grant No. 08040, and the Research Fund of the State Key Laboratory of Solidification Processing (NWPU), China (Grant No. 142-TZ-2016 and 98-QZ-2014).

References

[1] L. Zhuang, Q.G. Fu, B.Y. Tan, Y.A. Guo, Q.W. Ren, H.J. Li, B. Li, J.P. Zhang, Ablation behaviour of C/C and C/C-ZrC-SiC composites with cone-shaped holes under an oxyacetylene flame, Corros. Sci. 102 (2016) 84-92.

[2] N.S. Jacobson, D.M. Curry, Oxidation microstructure studies of reinforced carbon/carbon, Carbon. 44 (2006) 1142-1150.

[3] Y.L. Zhang, T. Fei, W.Y. Zeng, B.X. Yang, H.J. Li, K.Z. Li, Microstructure and oxidation behavior of C/C-ZrB_2-SiC composites coated with SiC coating at high temperature, Corros. Sci. 100 (2015) 421-427.

[4] F.L. Zhao, Q.G. Fu, L. Feng, Q.L. Shen, Enhancement of C/C-LAS joint using aligned carbon nanotubes prepared by injection chemical vapor deposition, Mater. Sci. Eng A. 650 (2016) 67-74.

[5] Y.L. Zhang, J.C. Ren, S. Tian, H.J. Li, X.R. Ren, Z.X. Hu, HfC nanowire-toughened $TaSi_2$-TaC-SiC-Si multiphase coating for C/C composites against oxidation, Corros. Sci. 90 (2015) 554-561.

[6] J.P. Zhang, Q.G. Fu, J.L. Qu, R.M. Yuan, H.J. Li, Blasting treatment and chemical vapor deposition of SiC nanowires to enhance the thermal shock resistance of SiC coating for carbon/carbon composites in combustion environment, J. Alloy and Compd. 666 (2016) 77-83.

[7] Y. Jia, K.Z. Li, L.Z. Xue, J.J. Ren, S.Y. Zhang, X.M. Zhang, Microstructure and mechanical properties of carbon fiber reinforced multilayered $(PyC\text{-}SiC)_n$ matrix composites, Mater Des. 86 (2015) 55-60.

[8] L.Z. Xue, K.Z. Li, Y. Jia, S.Y. Zhang, J.J. Ren, Z.Y. You, Effects of hypervelocity impact on ablation behavior of SiC coated C/C composites, Mater. Des. 108 (2016) 151-156.

[9] Q.G. Fu, J.Y. Jing, B.Y. Tan, R.M. Yuan, L. Zhuang, L. Li, Nanowire-toughened transition layer to improve the oxidation resistance of SiC-$MoSi_2$-ZrB_2 coating for C/C composites, Corros. Sci. 111 (2016) 259-266.

[10] Y. Liu, Q.G. Fu, J.P. Zhang, L. Li, L. Zhuang, Erosion resistance of C/C-SiC-ZrB_2 composites exposed to oxyacetylene torch, J Eur Ceram Soc. 36 (2016) 3815-3821.

[11] Q.G. Fu, H.J. Li, K.Z. Li, X.H. Shi, M. Huang, A $MoSi_2$-SiC-Si/glass oxidation protective coating for carbon/carbon composites, Carbon. 44 (2006) 3361-3364.

[12] K.Z. Li, D.S. Hou, H.J. Li, Q.G. Fu, G.S. Jiao, Si-W-Mo coating for SiC coated carbon/carbon composites against oxidation, Surf. Coat. Tech. 201 (2007) 9598-9602.

[13] S.A. Chen, C.R. Zhang, Y.D. Zhang, H.F. Hu, Preparation and properties of carbon fiber reinforced ZrC-ZrB_2 based composites via reactive melt infiltration, Compos Part B-Eng. 60 (2014) 222-226.

[14] M.M. Opeka, I.G. Talmy, J.A. Zaykoski, Oxidation-based materials selection for 2000+ hypersonic aerosurfaces: Theoretical considerations and historical experience, J. Mater. Sci. 39 (2004) 5887-5904.

[15] R.J. He, X.H. Zhang, P. Hu, W.B. Han, C.Q. Hong, Preparation of YAG gel coated ZrB_2-SiC composite prepared by gelcasting and pressureless sintering, Compos Part B-Eng. 54 (2013) 307-312.

[16] I.G. Talmy, J.A. Zaykoski, M.M. Opeka, High-temperature chemistry and oxidation of ZrB_2 ceramics containing SiC, Si_3N_4, Ta_5Si_3, and $TaSi_2$, J. Am. Ceram. Soc. 91 (2008) 2250-2257.

[17] I.G. Talmy, J.A. Zaykoski, M.M. Opeka, Oxidation of ZrB_2 ceramics modified with SiC and group IV-VI transition metal diborides, Elec. Chem. Soc. Proc. 12 (2001) 144-158.

[18] N. Akçamlı, D. A ğaoğulları, Ö. Balcı, Mechanical activation-assisted au toclave processing and sintering of HfB_2-HfO_2 ceramic powders, Ceram. Int. 42 (2016) 14642-14655.

[19] R.J. He, X.H. Zhang, W.B. Han, P. Hu, C.Q. Hong, Effects of solids loading on microstructure and mechanical properties of HfB_2-20 vol.% $MoSi_2$ ultra high temperature ceramic composites through aqueous gelcasting route, Mater. Des. 47 (2013) 35-40.

[20] Y. Ye, J.X. Liu, G.J. Zhang, Effect of HfC and SiC on microstructure and mechanical properties of HfB_2-based ceramics, Ceram. Int. 42(2016) 7861-7867.

[21] X.R. Ren, H.J. Li, Q.G. Fu, Y.H. Chu, K.Z. Li, TaB_2-SiC-Si multiphase oxidation protective coating for SiC-coated carbon/carbon composites, J. Eur. Ceram. Soc. 33 (2013) 2953-2959.

[22] H. Wu, H.J. Li, C. Ma, Q.G. Fu, Y.J. Wang, J.F. Wei, J. Tao, $MoSi_2$-based oxidation protective coatings for SiC-coated carbon/carbon composites prepared by supersonic plasma spraying, J. Eur. Ceram. Soc. 30 (2010) 3267-3270.

[23] Y.L. Zhang, H.J Li, X.F. Qiang, K.Z. Li, S.Y. Zhang, C/SiC/$MoSi_2$-Si multilayer coatings for carbon/carbon composites for protection against oxidation, Corros. Sci. 53 (2011) 3840-3844.

[24] Q.G. Fu, H.J. Li, Y. J. Wang, K.Z. Li, X.H. Shi, B_2O_3 modified SiC-$MoSi_2$ oxidation resistant coating for carbon/carbon composites by a two-step pack cementation, Corros. Sci.51 (2009) 2450-2454.

[25] B.L. Zou, Y. Hui, W.Z. Huang, S.M. Zhao, X.L.Chen, J.Y. Xu, Oxidation protection of carbon/carbon composites with a plasma-sprayed ZrB_2-SiC-Si/Yb_2SiO_5/$LaMgAl_{11}O_{19}$ coating during thermal cycling, J. Eur. Ceram. Soc. 35 (2015) 2017-2025.

[26] L. Zhuang, Q.G. Fu, Bonding strength, thermal shock and oxidation resistance of interlocking (Zr,Hf)C-SiC/SiC double-layer coating for C/C composites, Surf. Coat. Tech. 315 (2017) 436-442.

[27] S. Shimada, T. Sato, Preparation and high temperature oxidation of SiC compositionally graded graphite coated with HfO_2, Carbon. 40 (2002) 2469-2475.

[28] S. Shimada, T. Sato, High-Temperature Oxidation at 1500° and 1600°C of SiC/Graphite Coated with Sol-Gel-Derived HfO_2, J. Am. Ceram. Soc. 88 (2005) 845-849.

Figure captions

Fig.1 Illustration diagram of the preparation of the outer HfB_2-SiC-$MoSi_2$ coating;

Fig.2 XRD pattern of the outer HfB_2-SiC-$MoSi_2$ coating;

Fig.3 (a) Low magnification and (b) high magnification backscatter micrographs of the HfB_2-SiC-$MoSi_2$ coating; (c) spot EDS analyses of (b);

Fig.4 (a) Low and (b) high magnification cross-section backscatter micrographs of the coated C/C composites; (c) high magnification backscatter micrograph of the interface between C/C composites and the inner SiC layer; (d) magnification of part A in Fig.4 (a); (e) spot EDS analyses of Fig.4 (d); (f) EDS element line analyses of the coating;

Fig.5 Isothermal oxidation of the coated C/C composites in air at 1773 K;

Fig.6 XRD pattern of the double layer coated C/C composites after oxidation at 1773 K in air for 408 h;

Fig.7 (a) Surface backscatter micrograph of the double layer coated C/C composites after oxidation at 1773 K in air for 408 h; (b) magnification of part A in Fig.7 (a); (c) magnification of part B in Fig.7 (a); (d) spot EDS analyses of (b);

Fig.8 (a) Low and (b) high magnification cross-section backscatter micrograph of the coated C/C composites after oxidation; (c) magnification of part A in Fig.8 (b); (d) magnification of part B in Fig.8 (a); (e) magnification of part C in Fig.8 (a); (f) spot EDS analyses of Fig.8 (b) and (d);

Fig.9 TGA curves of coated C/C composites from room temperature to 1673 K;

Fig.10 Oxidation protection schematic diagram of the HfB_2-SiC-$MoSi_2$/SiC coating for C/C composites.

Figures

Fig.1

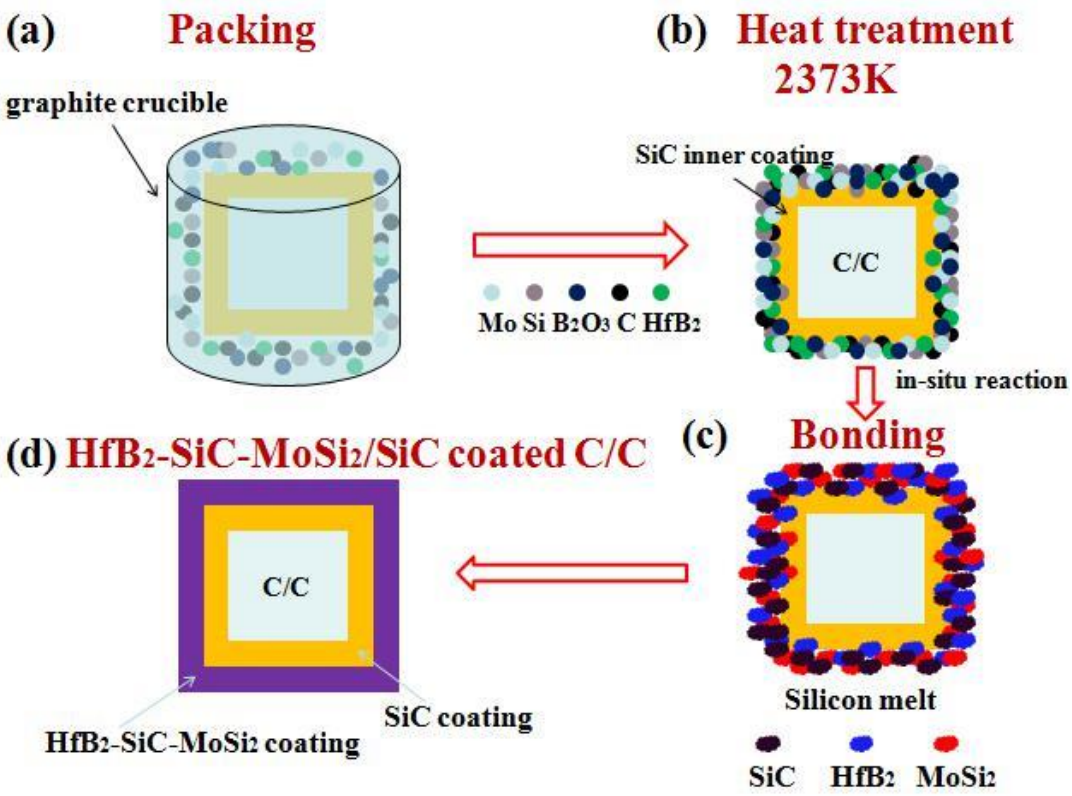

Fig.2

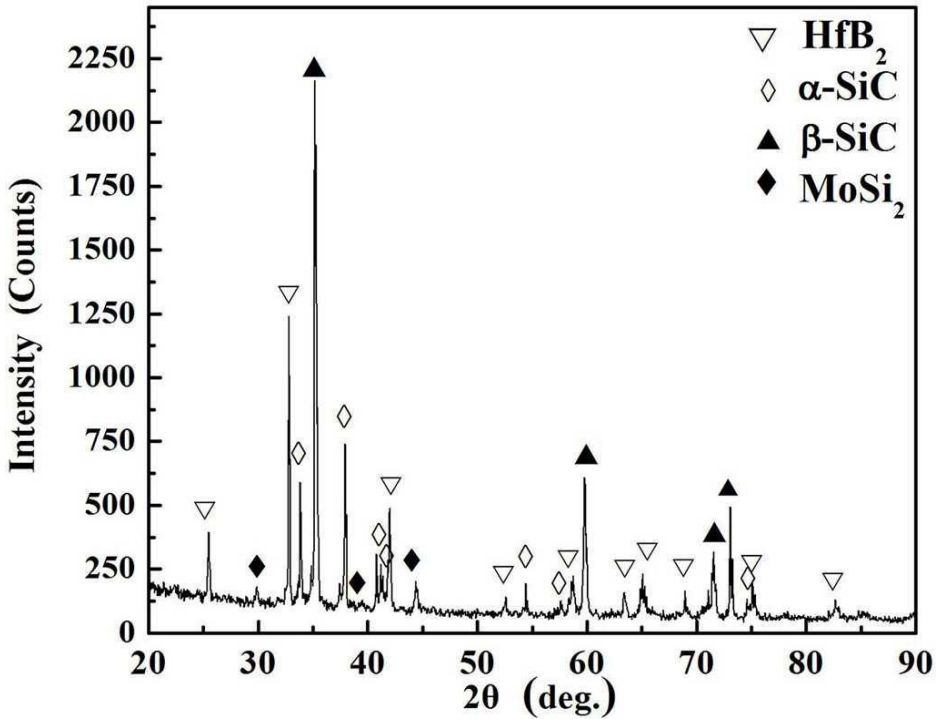
HfB2
α-SiC
β-SiC
MoSi2
Intensity (Counts)
2θ (deg.)
0
250
500
750
1000
1250
1500
1750
2000
2250
20
30
40
50
60
70
80
90

Fig.3

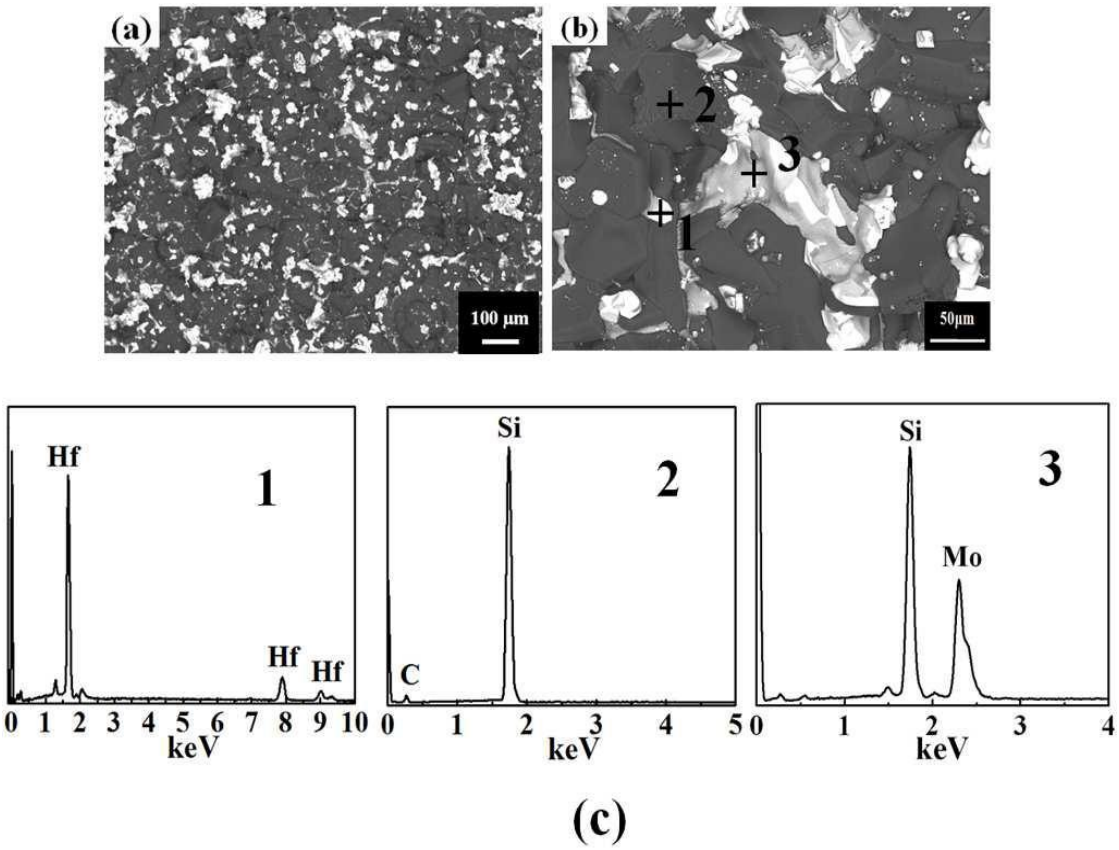
(a)
100 μm
(b)
+2
+3
+1
50μm
Hf
1
Hf
Hf
0 1 2 3 4 5 6 7 8 9 10
keV
Si
2
C
0 1 2 3 4 5
keV
Si
3
Mo
0 1 2 3 4
keV

(c)

Fig.4

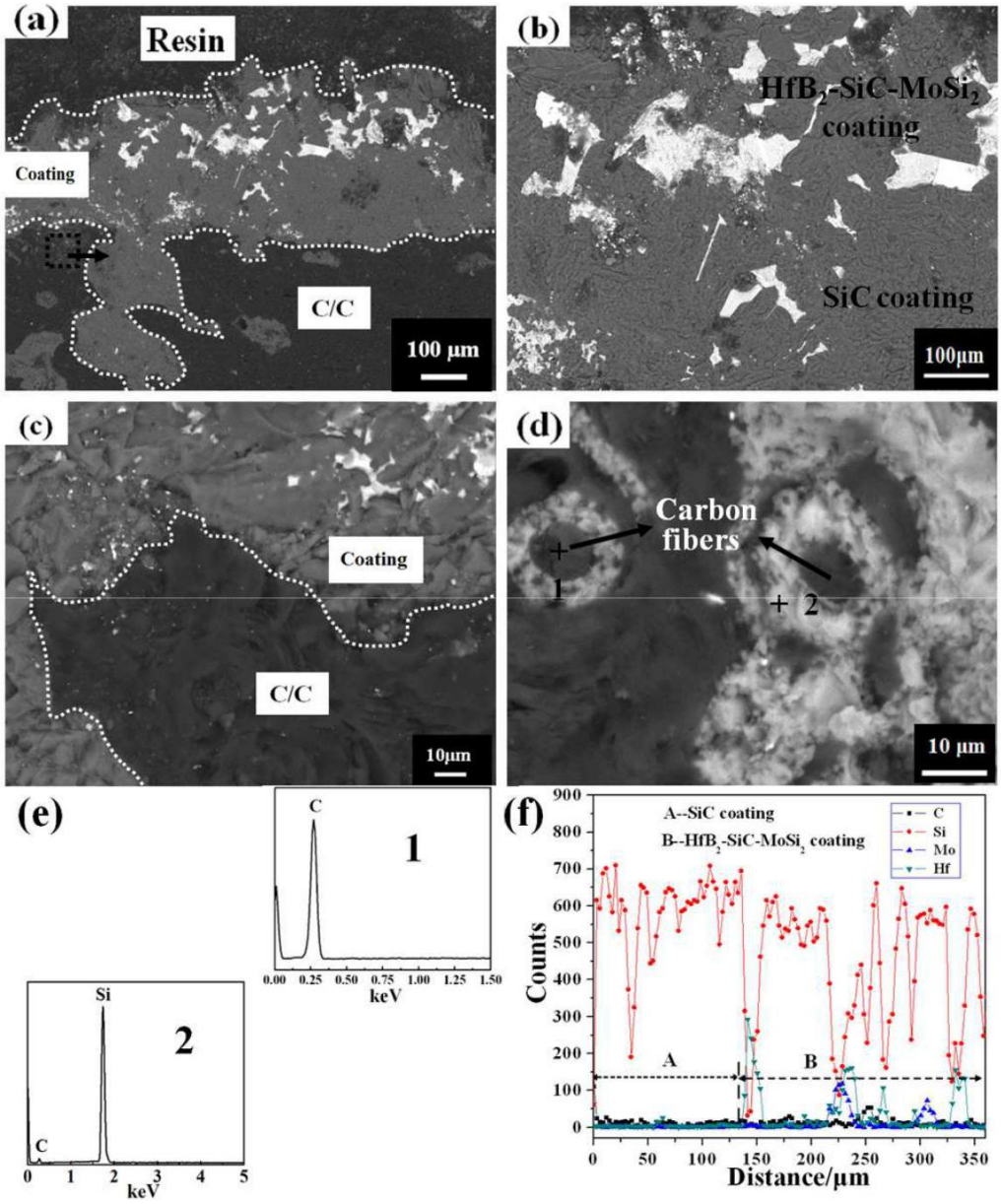
(a)
Resin
Coating
C/C
100 μm
(b)
HfB2-SiC-MoSi2 coating
SiC coating
100μm
(c)
Coating
C/C
10μm
(d)
Carbon fibers
1
2
10 μm
(e)
C
1
0.00 0.25 0.50 0.75 1.00 1.25 1.50
keV
Si
2
C
0 1 2 3 4 5
keV
(f)
A--SiC coating
B--HfB2-SiC-MoSi2 coating
C
Si
Mo
Hf
Counts
A
B
0 50 100 150 200 250 300 350
Distance/μm

Fig. 5

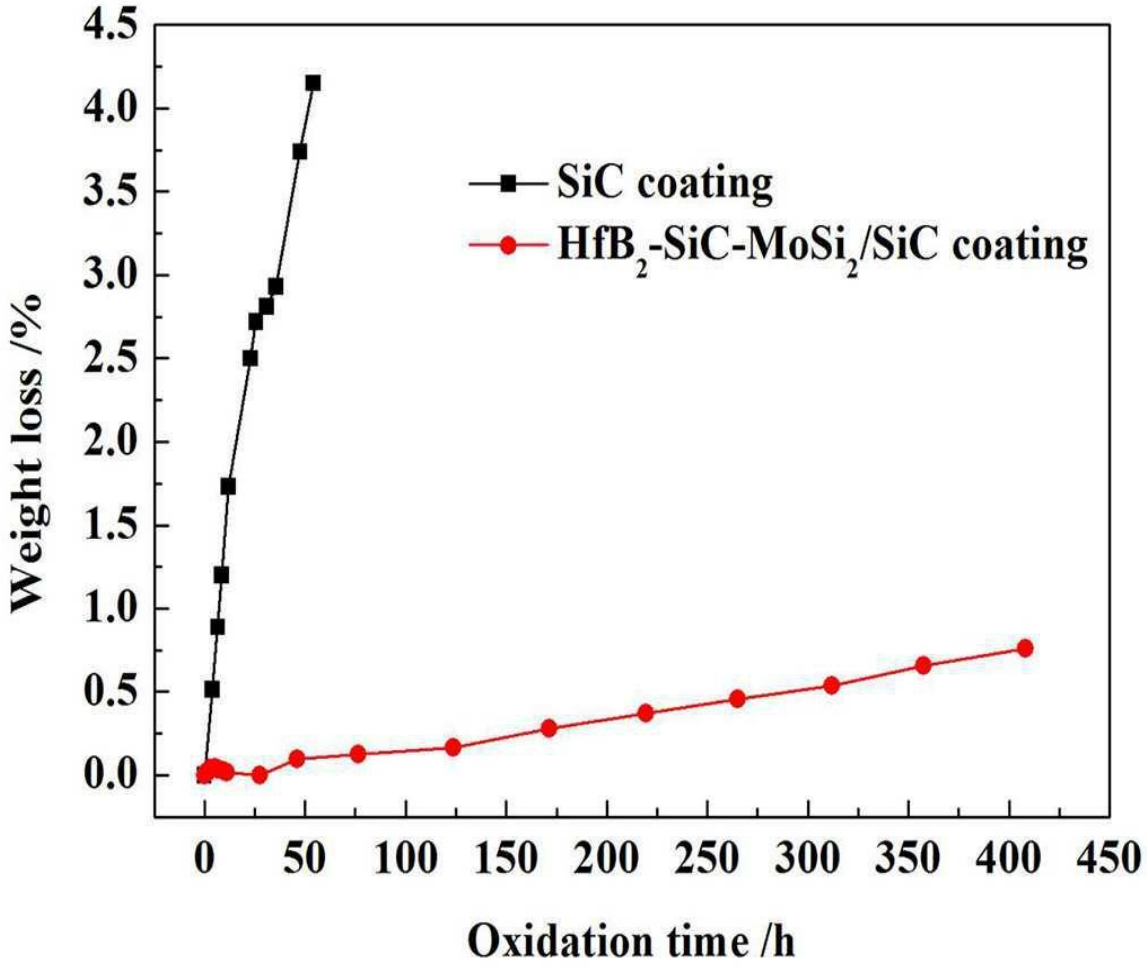
Weight loss /%
Oxidation time /h
SiC coating
HfB2-SiC-MoSi2/SiC coating
0.0
0.5
1.0
1.5
2.0
2.5
3.0
3.5
4.0
4.5
0
50
100
150
200
250
300
350
400
450

Fig. 6

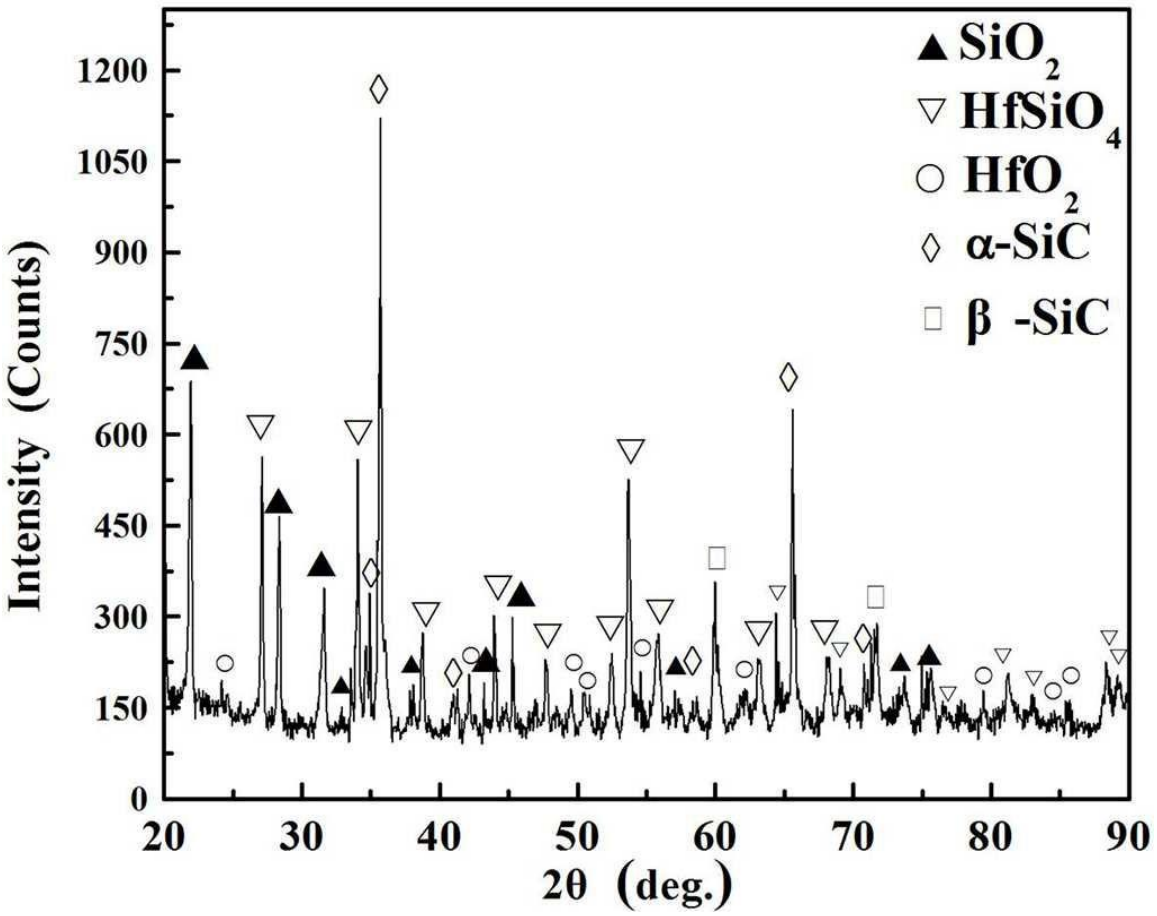
▲ SiO2
▽ HfSiO4
○ HfO2
◊ α-SiC
□ β -SiC
Intensity (Counts)
0
150
300
450
600
750
900
1050
1200
20
30
40
50
60
70
80
90
2θ (deg.)

Fig.7

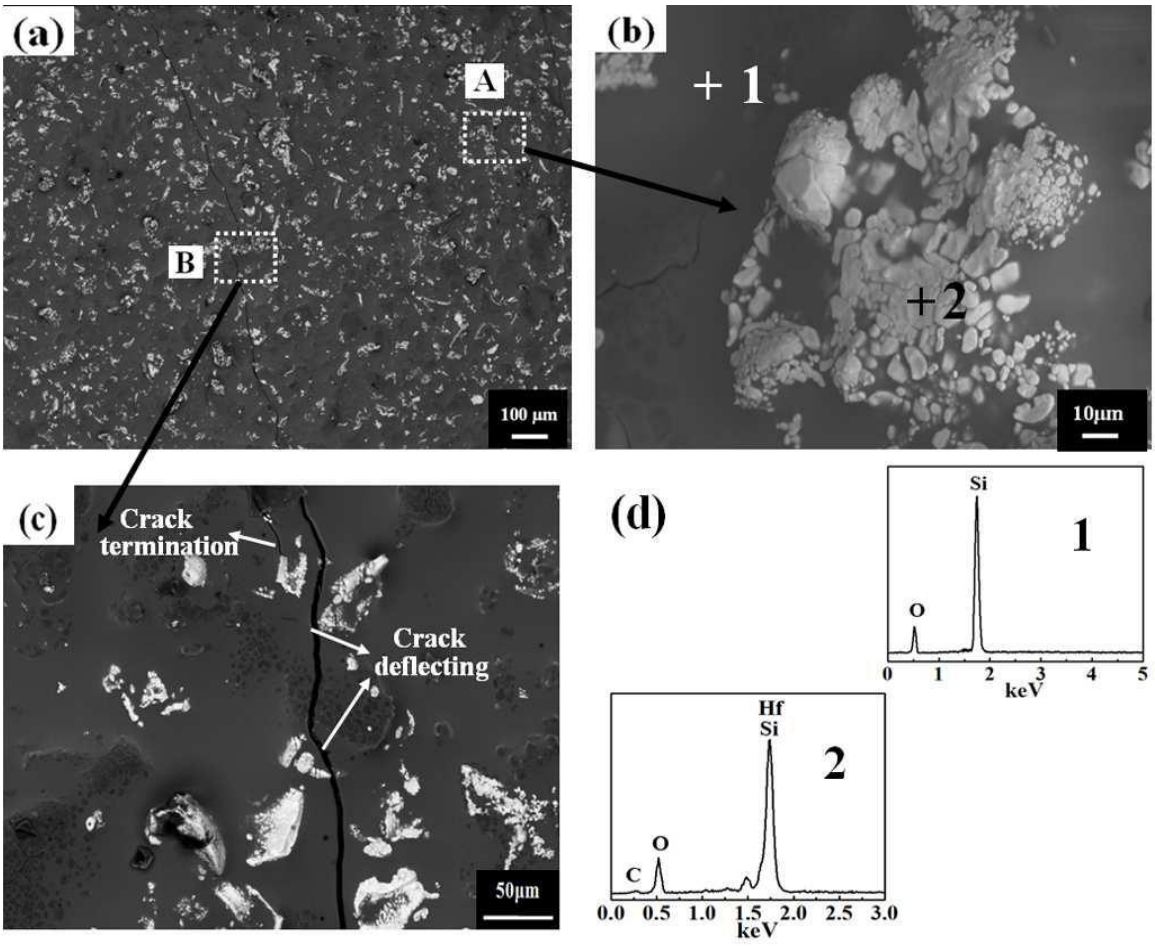
(a)
A
B
100 μm
(b)
+ 1
+2
10μm
(c)
Crack termination
Crack deflecting
50μm
(d)
Si
1
O
0 1 2 3 4 5
keV
Hf
Si
2
O
C
0.0 0.5 1.0 1.5 2.0 2.5 3.0
keV

Fig.8

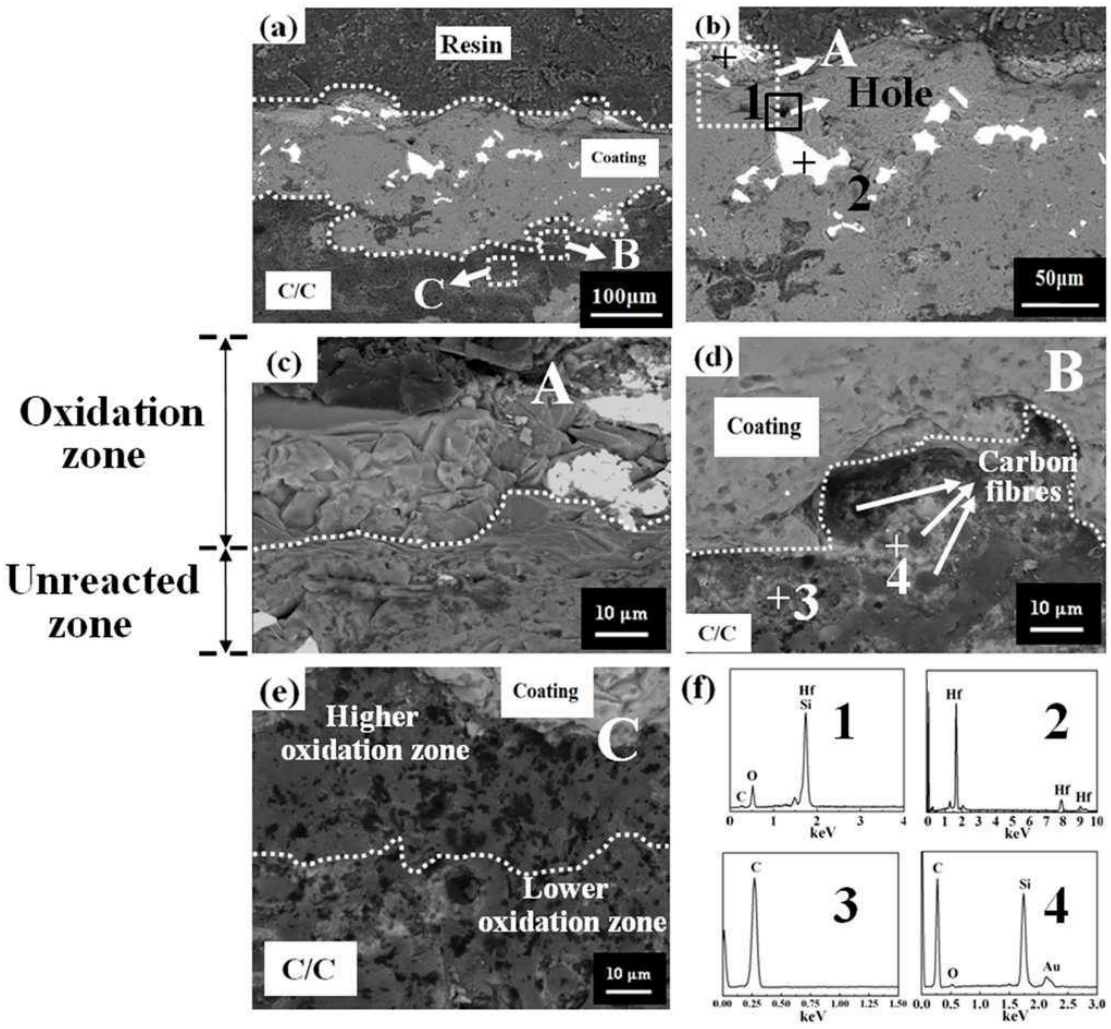
(a)
Resin
Coating
C/C
B
C
100μm
(b)
A
Hole
1
2
50μm
Oxidation zone
Unreacted zone
(c)
A
10 μm
(d)
B
Coating
Carbon fibres
4
3
C/C
10 μm
(e)
Coating
Higher oxidation zone
C
Lower oxidation zone
C/C
10 μm
(f)
Hf
Si
O
C
1
keV
Hf
2
Hf
Hf
keV
C
3
keV
C
Si
4
O
Au
keV

Fig.9

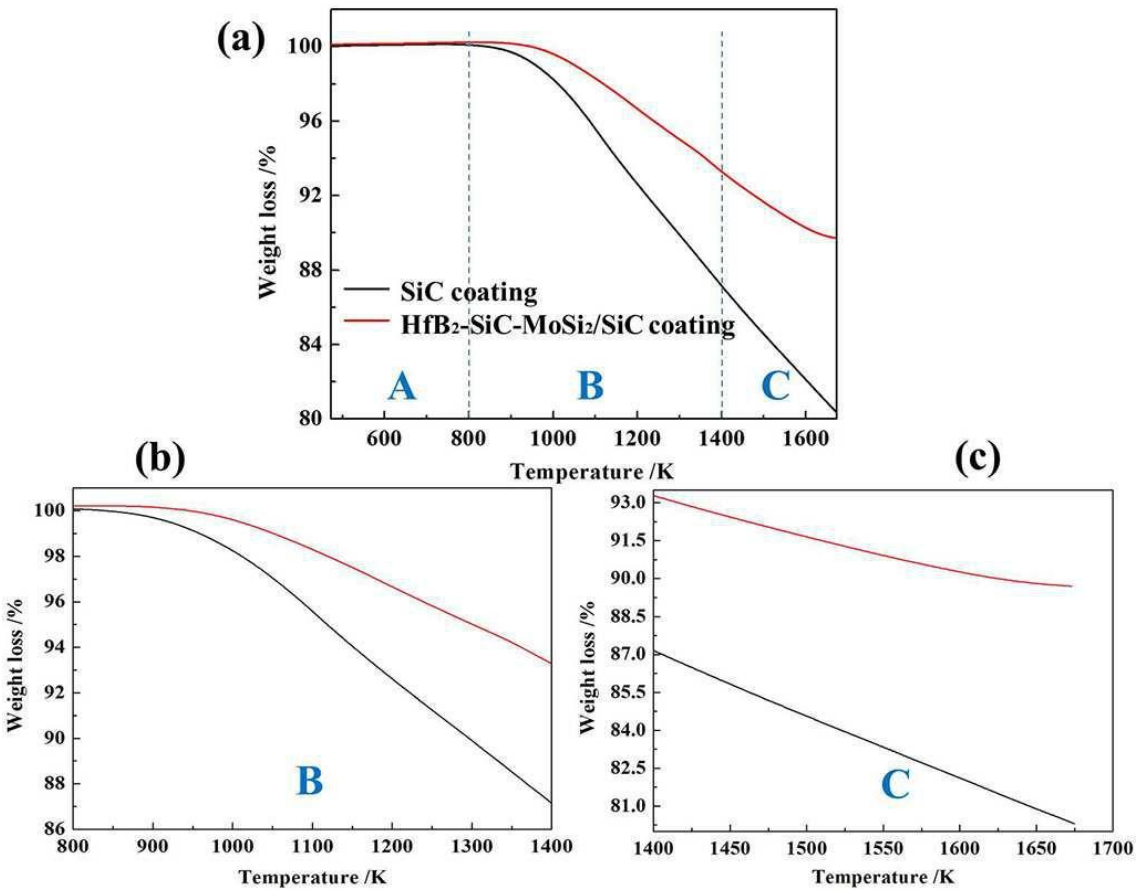
(a)
Weight loss /%
Temperature /K
SiC coating
HfB2-SiC-MoSi2/SiC coating
A
B
C
(b)
Weight loss /%
Temperature /K
B
(c)
Weight loss /%
Temperature /K
C

Fig.10

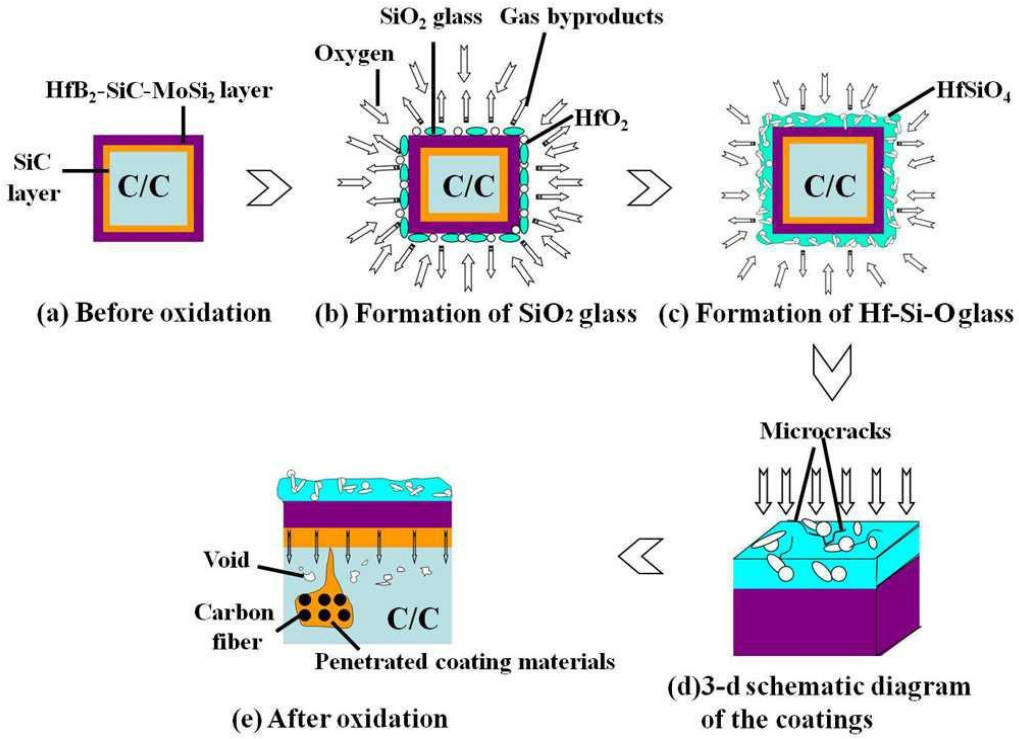
SiO_2 glass
Gas byproducts
Oxygen
HfB_2-SiC-$MoSi_2$ layer
HfO_2
$HfSiO_4$
SiC layer
C/C
C/C
C/C
(a) Before oxidation
(b) Formation of SiO_2 glass
(c) Formation of Hf-Si-O glass
Microcracks
Void
Carbon fiber
C/C
Penetrated coating materials
(e) After oxidation
(d)3-d schematic diagram of the coatings

Highlights

1. The UHTCs HfB_2-SiC-$MoSi_2$ coating was fabricated through in-situ synthesis.

2. The coating could protect C/C for 408 h with only 0.76% mass loss in 1773K air.

3. The SiO_2 glass layer offered the expected self-cure ability.

4. The Hf-Si-O glass layer was responsible for the good oxidation resistance.